International Journal of Thermofluids 28 (2025) 101321

Contents lists available at ScienceDirect

International Journal of Thermofluids

journal homepage: www.sciencedirect.com/journal/international-journal-of-thermofluids

Analysis of flow characteristics around sharp, blunt, and bulb-shaped missile nose geometries

Shamitha Shetty [a], Kavana Nagarkar [b], Sher Afghan Khan [c], Abdul Aabid [d,*], Muneer Baig [d]

[a] Department of Mathematics, Nitte Meenakshi Institute of Technology, Nitte (Deemed to be University), Bangalore 560064, Karnataka, India
[b] Department of Aeronautical Engineering, Nitte Meenakshi Institute of Technology, Nitte (Deemed to be University), Bangalore 560064, Karnataka, India
[c] Department of Mechanical and Aerospace Engineering, Faculty of Engineering, International Islamic University Malaysia, P.O. Box 10, 50725 Kuala Lumpur, Malaysia
[d] Department of Engineering Management, College of Engineering, Prince Sultan University, PO BOX 66833, Riyadh 11586, Saudi Arabia

ARTICLE INFO

Keywords:
Computational fluid dynamics (CFD)
Supersonic flow
Nose cone geometry
Shock wave interaction
Missile aerodynamics
Drag reduction

ABSTRACT

The current study investigates the aerodynamic characteristics of three distinct missile nose cone geometries: sharp, blunt, and bulb-shaped under supersonic conditions at Mach numbers 2.4, 2.8, 3.2, and 3.6. The primary objective is to analyze key parameters, such as lift and drag coefficients, and compare the findings with values reported in existing literature. The research aims to explore the flow physics responsible for variations in drag force as the missile nose shape is altered. Supersonic missile design has drawn significant interest, with improving performance remaining a critical focus for researchers and engineers. One of the main challenges in achieving better performance is mitigating the high drag forces experienced at these speeds. The research employs two-dimensional computational fluid dynamics simulations using the standard k-epsilon turbulence model in ANSYS Fluent. Key parameters such as drag coefficient, lift coefficient, and pressure distribution are analyzed to understand the impact of nose shape on aerodynamic efficiency. Results indicate that the sharp nose geometry exhibits significantly reduced drag compared to the blunt and bulb configurations due to streamlined shock wave interactions and reduced pressure concentration at the nose tip. Conversely, while producing higher drag, the blunt shape offers better heat dissipation potential due to increased surface exposure. This study fills a gap in the literature by conducting a detailed comparative analysis of unconventional nose shapes at high Mach numbers. The findings contribute to improved missile nose design by balancing drag reduction and thermal management in high-speed flight regimes. The study concludes that minimizing the missile's exposed surface area to the free-stream and shock interactions effectively reduces drag, as smaller surface areas diminish shock interaction and associated drag forces.

1. Introduction

Missile nose cone design determines aerodynamic performance, especially at supersonic and hypersonic speeds. Supersonic missile design requires precise control over aerodynamic forces, with nose cone geometry playing a pivotal role in minimizing drag and managing thermal loads. Nose cone geometry significantly influences key aerodynamic parameters, including drag, lift, pressure distribution, and shock wave dynamics. The interaction between the shock waves and the missile surface at higher Mach numbers becomes more pronounced, leading to increased aerodynamic heating and potential material degradation at the nose tip.

Among the many challenges in supersonic missile design are the high drag forces generated by shock interactions and flow separation and the thermal loads caused by stagnation heating. Reducing these aerodynamic penalties while maintaining structural integrity is essential to improving overall missile efficiency.

Traditional studies have predominantly focused on conical and ogive profiles under subsonic conditions. However, there remains a need to evaluate unconventional shapes such as blunt and bulb-shaped noses under supersonic flow to balance aerodynamic efficiency and thermal resilience.Recent work, however, has begun to explore more complex geometries, such as bulbous or blunted shapes and their behavior at supersonic speeds. For instance, studies by Kim and Al-Obaidi [1], Nagaharish et al. [2], and Dash et al. [3] have emphasized the need for optimized geometries that strike a balance between drag reduction and thermal management.

* Corresponding author.
E-mail address: aaabid@psu.edu.sa (A. Aabid).

https://doi.org/10.1016/j.ijft.2025.101321

Available online 28 June 2025

Nomenclature

RANS	Reynolds Averaged Navier-Stokes Equations
Cd	Coefficient of drag
CFD	Computational fluid dynamics
Cl	Coefficient of lift
M_∞	Freestream Mach number
P_∞ (Pa)	Freestream pressure
T_∞ (K)	Freestream temperature
Re_∞ (million/m)	Freestream Reynolds number
U_∞ (m/s)	Freestream velocity
Tw (K)	Wall temperature

Despite these advancements, comparative data remains on how non-conventional shapes, particularly bulbous noses, perform in the supersonic regime. This study addresses this gap by numerically analyzing and comparing three missile nose geometries (sharp, blunt, and bulb-shaped) under identical freestream conditions. This work uses CFD simulations to evaluate aerodynamic coefficients and flow features, offering design insights relevant to supersonic missile applications. The novelty lies in exploring how shock wave formation and pressure gradients vary with each geometry, providing deeper insight into supersonic missile nose design and exploring how shock wave formation and pressure gradients vary with each geometry, providing deeper insight into supersonic missile nose design.

Through many computational fluid dynamics (CFD) analyses and research, it's been concluded that the missile with a very sharp, pointy nose experiences less drag than others, which exposes more area to free stream. However, at higher supersonic speeds, a sharp-pointed nose cone is prone to rapid heating due to continuous aerodynamic drag. As the area exposed is less, the transfer of heat becomes complex, and the temperature at the point starts to rise, eventually causing the melting of material or absolute destruction of the missile. Therefore, the proper comparative analysis for different nose cone geometries at supersonic speed is necessary. Many works have been done on comparing the same using other geometries, as explained in the literature survey's later section.

2. Related work

Numerous studies have addressed the aerodynamic performance of various missile nose geometries under subsonic, transonic, and supersonic conditions. Traditional geometries such as conical and ogive nose cones have been widely analyzed for their influence on drag and lift. Kumar [4] compared conical and tangent ogive profiles and observed a lower drag coefficient for the latter. Similarly, Sreenivasula Reddy [5] performed structural analysis of nose cones with different materials, highlighting the advantages of titanium alloys under high thermal loads. Using ANSYS FLUENT software, Kumar [4] analyzes two different missile nose cone profiles, namely the conical and tangent ogive shapes. The study examines the variations in drag and lift forces and the pressure and velocity contours around these nose cone models at various Mach numbers. The results reveal that the tangent ogive nose cone has a lower drag coefficient than the conical nose cone, indicating reduced drag and aerodynamic heating. This makes the tangent of the nose cone more efficient for supersonic applications. The work by Sreenivasula Reddy [5] focuses on the design and structural analysis of missile nose cones using different materials, including Titanium alloys (Ti-6Al-4V, Ti-6Al-6V-2SN, and Titanium Grade 1).

More recent research has explored complex flow interactions and the effects of angle of attack (AoA) on missile stability. Gaonkar et al. [6] and Divakaran et al. [7] numerically analyzed missile aerodynamics at various AoA, reporting variations in lift-to-drag ratios. These studies have emphasized the critical importance of shape optimization in supersonic flight regimes. However, relatively few studies have addressed bulb-shaped nose cones at supersonic speeds or compared them directly to sharp and blunt configurations. Additionally, existing literature often lacks validation against consistent freestream conditions and fails to consider both aerodynamic and thermal implications simultaneously.

This research attempts to bridge this gap by performing a comparative CFD study on three distinct geometries (sharp, blunt, and bulb) using identical supersonic freestream conditions. Focusing on Mach numbers between 2.4 and 3.6, this study extends previous work into a higher speed regime where compressibility and shock wave effects dominate. It also contributes to understanding how unconventional nose geometries influence aerodynamic behavior, pressure distribution, and shock wave formation.

The research involves modeling missile nose cones using CATIA software and conducting structural analysis using ANSYS to evaluate the effects of air pressure and temperature at high altitudes. Two nose cone designs were analyzed under static conditions to compare their deformation, stress, and strain characteristics. The results indicate that the Titanium Ti-6Al-4V alloy offers superior performance with minimal deformation and weight, making it the most suitable material for missile nose cones compared to other materials like aluminum and stainless steel. Ashwini Anand Gaonkar [6] focuses on optimizing the aerodynamic performance of a supersonic missile using numerical simulations. The study specifically explores the impact of varying the angle of attack, ranging from 0° to 12°, while keeping the Mach number constant at 2.5. Using ANSYS FLUENT for flow analysis, the missile's performance was evaluated by analyzing key parameters like lift and drag coefficients. The results revealed that increasing the angle of attack improved the aerodynamic efficiency, with the highest coefficient of lift-to-drag ratio (Cl/Cd) of 2.5 observed at a 12° angle of attack. The study concluded that higher angles of attack enhance the missile's aerodynamic efficiency, providing valuable insights for missile design optimization.

Raghuvaran Divakaran [7] explores the aerodynamic performance of the V-2 missile using numerical simulations. The authors use ANSYS software to model the missile and analyze the effects of various angles of attack, ranging from 0° to 16°, and Mach numbers between 2 and 3.5. The study investigates parameters such as density, static temperature, pressure coefficient, and Mach number. The simulations reveal that as the angle of attack increases, drag and friction also rise, affecting the missile's overall aerodynamic performance. Despite these increases, the missile maintains aerodynamic efficiency even at higher angles, ensuring stable flight at high velocities. The results contribute valuable insights for enhancing the missile's design and performance under supersonic conditions. Pandie [8] examines a guided missile's aerodynamic characteristics using CFD (ANSYS R15.0) software. The researchers focus on simulating the fluid flow around a SCUD missile to observe how variations in the angle of attack (α) from 0° to 15° impact pressure, velocity, lift, and drag. Using CATIA to model the missile and ANSYS for simulations, they analyzed key aerodynamic parameters. The results showed that lift and drag rose significantly as the angle of attack increased. This research provides valuable insights into missile design and performance, demonstrating that greater angles of attack generate higher pressure and lift, improving missile stability and control. The journal, by Janine Schoombie [9], presents a combined experimental and computational analysis of a slender body with low aspect ratio wings at low Mach numbers. The study investigates aerodynamic loads and flow features, showing a good correlation between CFD simulations and experimental data for angles of attack above 6 degrees. Vortex separation was observed, suggesting configuration-specific flow phenomena with no Mach number dependency on the global loads.

Using CFD simulations, Srinivas and Prakash [10] explore the aerodynamics and flow characteristics of single, double, and multistage rockets. The study optimizes rocket designs for efficient stage separation and performance under varying Mach numbers. It concludes that while

Mach speed 3 provides optimal results for staging, Mach speed six can be feasible for triple-stage rockets, offering better aerodynamic performance due to lower shock wave intensity at the nose. The journal article by Jubaraj Sahu and Karen R. Heavy [11] focuses on CFD simulations of a finned projectile's aerodynamics with and without flow control using microflaps. The study employs advanced Navier-Stokes equations to predict aerodynamic forces at various speeds. The authors conclude that microflaps are ineffective at transonic speeds but provide significant control forces at supersonic velocities, offering the potential for enhanced maneuverability in projectiles. The journal article by Goran Ocokoljić focuses on optimizing the aerodynamic shape of guided missiles using wind tunnel tests and CFD simulations. The study modifies missile designs by replacing the front part to enhance aerodynamic performance while maintaining the original rear. They concluded that the new configurations, notably the 2FF model, improved the lift-to-drag ratio and aerodynamic characteristics, demonstrating the effectiveness of optimization. Devendra [12] discusses the design and structural analysis of missile nose cones using materials such as Titanium Grade-I, Ti-6Al-4V, and Ti-6Al-6V-2Sn. The study used CAD software (CATIA) and structural analysis software (ANSYS). The authors concluded that Ti-6Al-4V showed the least deformation and was the most suitable material due to its high strength, low weight, and corrosion resistance.

Kim and Al-Obaidi investigated the influence of various nose shapes on missile performance at supersonic speeds, focusing on aerodynamic optimization. The findings indicated that specific geometries can significantly reduce drag and improve stability at high speeds. Similarly, Nagaharish examined fluid flow effects over rotating bodies with distinct nose cone shapes, concluding that geometry directly impacts aerodynamic efficiency. Seoeum Han compared calculation methods for nose shape deformations, aiming to refine models for enhanced missile stability and control. These studies collectively emphasize the critical role of nose cone geometry in optimizing supersonic missile performance. Y. Mohsen [13] conducted a study comparing supercavitating flow behavior over different projectile nose shapes. The results highlighted that hemispherical noses minimized drag in supercavitating environments, making them practical for underwater applications. Semih M. Ölçmen [14] team focused on achieving minimum drag and heating for projectiles with optimal nose geometries, finding that sharper, smaller noses best reduced both. Recently, Sambit Supriya Dash and team proposed a novel dimpled nose cone design for launch vehicles, showing that dimples improve stability across various speeds by altering flow patterns.

Narayan et al. [15–17] conducted a comparative study on hypersonic flow over different nose cone shapes, finding that parabolic geometries reduce drag and minimize aerodynamic heating due to favorable shock wave characteristics, making them ideal for high-speed applications. Khalghani [18,19] investigated the aerodynamic and flight dynamics of nine different missile configurations with deflectable noses. It finds that while increased flexibility and fixed part lengths improve maneuverability, these factors can sometimes reduce mission accuracy. A multi-block approach to solving Navier-Stokes equations and flight dynamics showed that geometric optimization must also account for flight dynamics and thrust vector control to improve accuracy. Kumar [20] explores wedge and cone nose profiles at supersonic speeds, examining shock wave effects and pressure distribution using theoretical and numerical analysis to optimize high-speed vehicle designs. Lopera [21] investigates the influence of forebody geometry on flow behavior for blunt-nosed projectiles at high angles of attack, emphasizing the critical role of shape in stability and performance.

Belega [22] employs CFD and SPH methods to optimize nose cone designs for missiles, focusing on improving aerodynamic efficiency and flight characteristics under varying conditions. The studies focus on aerodynamic and heat transfer phenomena in high-speed flow over various nose configurations. Gnemmi [23] examined spike-tipped bodies at high angles of attack, identifying flowfield behaviors and drag reduction mechanisms at Mach 4.5. Srulijes [24] explored heat transfer at the nose of high-speed missiles. Heydari [25] investigated supersonic flow around long axisymmetric bodies, focusing on shock-wave interactions and aerodynamic efficiency. Goyal [26] focused on the aerodynamic performance of supersonic and hypersonic missiles, analyzing their behavior under different flight conditions and emphasizing factors like stability and control at extreme speeds. Krieger [27] discussed the correlation of oil flow with aerodynamic properties in advanced missile concepts, utilizing oil flow visualization to study the effects of different body shapes on aerodynamic performance. These studies contribute to improving the understanding of missile flow dynamics, enhancing design predictions, and exploring the challenges faced at hypersonic speeds.

The simulation results aim to validate the experimental results of Sowoud et al. [28]. Suresh et al. [29] have determined the drag coefficient through simulations. They discovered the net drag coefficient (Cd). Still, they did not refer to the pressure coefficient, which is crucial for comparing the outcomes in this case, particularly for the base pressure and, consequently, the base drag. The simulation test is used by Sajali et al. [30] to determine the flow field and pressure coefficient (Cp) of the non-circular cylinder form. However, they only looked at the distance between the front body of a non-circular cylinder with 0 mm and 100 mm and the speed of 20.38 m/s. The author labels the non-circular cylinder's front body as 100 mm with pipe and 0 mm without pipe, respectively. The flow field is then displayed in terms of temperature, density, pressure, and Mach number. As a result, this study continues to confirm the Cp at a speed of 26.84 m/s and demonstrate the impact of the non-circular cylinder's front body distance. The efficiency of microjets in regulating the base pressure was determined [31] using a convergence-divergence nozzle with abrupt expansion and numerous studies has been performed for flow charaterization [32–37]. The parameters that the authors compared the experimental results with using the modeling results were the area ratio, length-to-diameter ratio, and NPR at different Mach numbers. Khan et al. used an ANSYS simulation to determine the supersonic flow over a delta wing [38–40].

3. Computation fluid dynamics

Considering the above, studies have shown that, under more excellent L/D circumstances, the forward-facing cavity mechanism considerably lowers drag over the nose surface. For the present work, the experiments by Kumar [18] have been considered a source of all the parameters and data with which numerical results are validated.

3.1. Governing equations

The methods and tools mentioned in Table 2 are used for the analysis. The software calculations are based on a theoretical formula or equation, the Navier-Stokes equation, which combines conservation equations (i.e., Continuity, momentum, and Energy equations). The Navier-Stokes equations for compressible flows account for changes in fluid density and involve additional terms to describe energy conservation. The equations are expressed in the following form (40,41):

Continuity Equation (Conservation of Mass):

$$\frac{\partial \rho}{\partial t} + \nabla.(\rho u) = 0 \tag{1}$$

where, ρis the density of the fluid, and u is the velocity vector.

Momentum Equation (Conservation of Momentum):

$$\frac{\partial (\rho u)}{\partial t} + \nabla.(\rho uu) = -\nabla p + \nabla.\tau + \rho f \tag{2}$$

where,

P is the pressure τ is the viscous stress tensor, which is represented as:

$$\tau = \mu\left(\nabla u + (\nabla u)^T\right) - \frac{2}{3}\mu(\nabla . u)I \tag{3}$$

where μ is the dynamic viscosity, and I is the identity matrix and f represents external forces (e.g., gravity).

Energy Equation (Conservation of Energy):

$$\frac{\partial(\rho e)}{\partial t} + \nabla.(\rho e u) = -\nabla.q + \tau : \nabla u + \rho f.u \tag{4}$$

where E is the total specific energy defined as the sum of internal energy e_{int} and kinetic energy.

$$\frac{1}{2}\ u.u$$

Q is the heat flux vector given by Fourier's law:

$$q = -k\nabla \mathrm{T} \tag{5}$$

where k is the thermal conductivity, and T is the temperature. These equations comprehensively describe compressible flows' behavior, capturing the interrelationships between mass, momentum, and energy conservation.

The current work, which focuses on finding the optimal missile nose cone shape for a missile with Mach number 2, follows the methods and methodology explained in the further section. Typically, it follows three steps of CFD processing: Preprocessing, Solver, and postprocessing.

The preprocessing involves conceptual design with collected data and meshing all geometries with proper dimensions. Mesh quality was assessed using metrics such as skewness and orthogonality to ensure simulation accuracy. Then, the solver step involves ANSYS Fluent solver with appropriate setup from solving model, implementation of input data, and obtaining result data from case setup. Further, the obtained results are best viewed and analyzed in CFD post, which comes under the postprocessing process.

3.2. Computational methodology

The aerodynamic performance of three missile nose cone geometries was analyzed using CFD simulations in ANSYS Fluent. A two-dimensional (2D) approximation was adopted to reduce computational cost while capturing the essential flow physics around axisymmetric nose shapes. This simplification is supported by prior studies which show that 2D simulations yield reasonably accurate results for symmetric bodies at zero angle of attack in supersonic flows.

The CFD methodology comprises three main phases: preprocessing (geometry creation and meshing), solution setup and computation, and postprocessing (data analysis and visualization). Geometries were modeled using ANSYS DesignModeler, and a large rectangular computational domain was created around each missile nose to simulate far-field atmospheric conditions.

High-quality structured meshes were generated using ANSYS Meshing Workbench, maintaining a skewness ratio below 0.1 and orthogonality above 0.9. Fine mesh refinement was better applied near the wall and nose tip to resolve the shock wave formation and boundary layer behavior. A mesh independence study was conducted to ensure that numerical results were not sensitive to mesh density.

3.3. Turbulence modelling

ANSYS Workbench is an engineering software suite with various solvers and project management utilities. This project's main toolbox is used for solving and postprocessing. ANSYS FLUENT is used as the solver for analysis purposes. ANSYS FLUENT uses unstructured meshes to reduce mesh generation time, simplify geometry modeling and mesh generation processes, and enable the modeling of more complex geometries than traditional multi-block structured meshes can handle. Adapt the mesh to solve the flow field features. ANSYS FLUENT can also use a block-structured mesh adapted to the body. ANSYS FLUENT can handle triangular and quadrilateral elements (or a combination of both) in 2D and tetrahedral, hexahedral, pyramidal, wedge-shaped, and polyhedral elements (or a combination thereof) in 3D In CFD, the Reynolds-Averaged Navier-Stokes (RANS) equations play a crucial role in simulating turbulent flows in ANSYS.

The Reynolds-Averaged Navier-Stokes (RANS) equations simulated the compressible, turbulent flow over the missile nose cones. Turbulence effects were modeled using the standard k-ε model, which provides robust and computationally efficient solutions for external aerodynamic flows. Although advanced models like the SST k-ω or Realizable k-ε with enhanced wall treatment are better suited for capturing near-wall behavior, the standard k-ε model was chosen due to its stability, broad applicability, and validation in previous missile nose flow studies. The focus on large-scale flow behavior and pressure drag justified this choice, and wall functions were used to approximate near-wall effects.

The fluid was treated as an ideal gas, and Sutherland's law was used to compute dynamic viscosity. Inviscid fluxes were calculated using the Advection Upstream Splitting Method (AUSM), with a Courant–Friedrichs–Lewy (CFL) number of 0.5. Boundary conditions comprised a pressure inlet and outlet, symmetry boundaries along the horizontal axis, and no-slip adiabatic walls along the nose surface.

These equations are a time-averaged version of the Navier-Stokes equations, the fundamental governing equations for fluid flow. By averaging the turbulent fluctuations, the RANS equations make it feasible to model complex, time-varying turbulent phenomena without resolving every small-scale eddy in the flow. That significantly reduces computational costs while providing accurate predictions for mean flow characteristics like velocity, pressure, and turbulence. In ANSYS, the RANS equations are used alongside turbulence models such as k-ε and k-ω, which provide additional closure relationships to solve turbulent stresses and ensure a complete set of solvable equations. This approach is widely applied in industries for simulations involving aerodynamic design, heat transfer, and fluid-structure interactions. The governing equations that are used to solve the flow physics of the blunt nose cone are Reynolds Averaged Navier-Stokes (RANS) equations, the Standard K-epsilon model, and the Sutherland 3-equation model was used to compute the viscosity over the blunt nose. The Advection Upstream Splitting Method (AUSM) scheme was used for inviscid flux calculations. A CFL number of 0.5 was maintained throughout the flow. The fluid is considered to be Ideal gas.

3.4. Problem definition

In the current work, three geometries with an increase in the exposure area are chosen for comparative study, i.e., sharp or pointed nose cone as case 1, blunt nose cone as case 2, and blub-shaped nose cone as case 3. All three geometries considered underwent the same

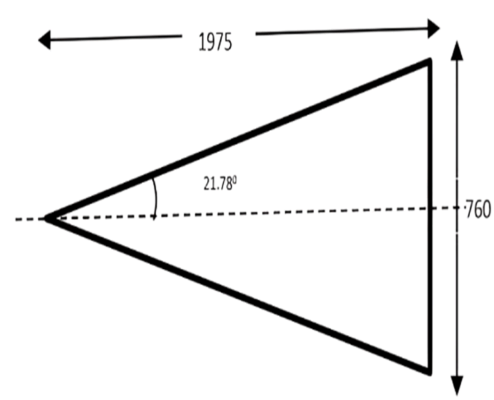

Fig. 1. Sharp nose cone for case-1 investigation.

methodology. The three geometries of the missile cones are shown in Figs. 1–3, with all the dimensions in mm.

The geometry of a missile's nose cone plays a decisive role in its aerodynamic efficiency and structural endurance, especially in supersonic flow regimes. While sharp nose cones typically produce lower drag due to minimal shock interaction, they are highly susceptible to thermal damage due to concentrated stagnation heating. On the other hand, blunt and bulbous shapes may reduce thermal loads but often introduce higher drag due to enhanced frontal area and shock intensity.

This study investigates three geometries with varying exposure areas: a sharp or pointed nose cone (Case 1), a blunt nose cone (Case 2), and a bulb-shaped nose cone (Case 3). These designs were selected based on their representation of familiar and novel profiles seen in missile applications. Although the physical dimensions of the geometries differ—Case 1 being significantly longer—the study aims to compare aerodynamic characteristics qualitatively and evaluate flow behavior trends.

The central objective is to analyze how each shape affects flow patterns, pressure concentration, lift, and drag under similar freestream Mach numbers (2.4 to 3.6). The simulations are conducted in a two-dimensional domain under the assumption of axial symmetry. The methodology and boundary conditions are kept constant across all geometries to isolate the effects of shape on performance.

Examining these nose shapes side-by-side, this study aims to offer insights for future missile design strategies that must balance drag minimization with heat load management.

The Mach number is constant for all three geometries to make comparison easy and accurate. The work by Gaurav Kumar [1] involves the CFD analysis of four different missile shapes, focusing on aerodynamic performance, particularly drag coefficient, under varying Mach numbers. Using CAD models and simulations in ANSYS, the researchers evaluated each missile's pressure, velocity, and boundary layer formation. They found that Case 3, a blend of other designs, had the lowest drag coefficient, making it the most optimized design. Case 4 had slightly higher drag but no flow separation, making it a promising alternative for smaller missiles. The study concludes that CFD is an effective tool for missile design, significantly reducing the need for physical experiments while optimizing aerodynamic performance. Figs. 1–3 serve as the problem definition, with dimensional information of nose shapes considered in these cases.

4. Finite volume method

4.1. Simulation model and boundary conditions

Table 2 brieflsy summarizes the methods and tools used throughout the process. The geometric dimensions are in mm, and the angles in degrees. The geometries are created using the ANSYS design modeler. The nose geometries are then bounded by a far-field or enclosure that acts like an atmosphere or free stream for the missile nose cone. After creating geometries with a considerable field, the meshing is done around the missile nose cone shapes. Figs. 4–6 show the geometries with boundary conditions.

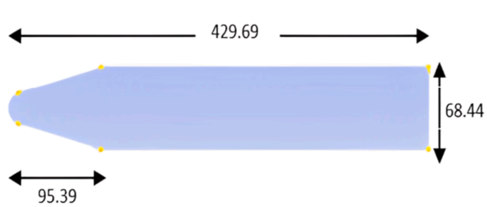

Fig. 2. Blunt nose for case-2 investigation.

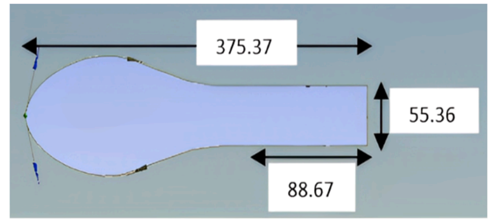

Fig. 3. Bulb-shaped nose for case-3 investigation.

4.2. Meshing and analysis

The meshing process in this study follows a rigorous approach to ensure the accuracy and reliability of numerical simulations. The meshes are designed with a skewness ratio of <0.1, ensuring optimal element quality. Structured grids with rectangular elements are generated in ANSYS Workbench, promoting uniformity in the distribution of elements and enabling accurate computation of flow parameters. Additionally, ANSYS Fluent employs unstructured meshes, allowing for efficient handling of complex geometries and reducing overall mesh generation time. The mesh structure comprises various element types, including triangular and quadrilateral elements in 2D, while 3D configurations incorporate tetrahedral, hexahedral, pyramidal, wedge-shaped, and polyhedral elements. This diversity in element types facilitates improved adaptability to intricate geometries and flow regions.

To enhance computational accuracy, the mesh is further refined based on flow features, particularly in high-gradient regions, ensuring a better resolution of governing equations. The simulation model mesh for different missile nose cone geometries is depicted in Figs. 7–9. These figures provide a detailed visualization of the meshing strategy adopted for various cases, with zoomed-in views emphasizing the fine mesh near the walls for improved accuracy in boundary layer resolution. The structured meshing approach ensures better convergence and precise prediction of aerodynamic characteristics.

The solver setup employs freestream conditions consistent across different geometries, with Mach numbers between 2.4 and 3.6, as detailed in Table 1. The freestream parameters include a pressure of 101,325 Pa, a temperature of 143 K, and velocity values corresponding to different Mach numbers (816 m/s for Mach 2.4, 952 m/s for Mach 2.8, 1088 m/s for Mach 3.2, and 1224 m/s for Mach 3.6). These conditions provide a realistic aerodynamic environment for analyzing flow characteristics.

Table 2 summarizes the methods and tools utilized in the computational framework. The methodology follows a systematic approach, beginning with mesh creation for all geometries in ANSYS Workbench, ensuring high-quality meshing through skewness and orthogonality checks. The solver setup is conducted in ANSYS Fluent, employing the standard k-epsilon turbulence model to capture the effects of turbulent flow. Postprocessing is performed using CFD-Post, where contour visualization techniques aid in understanding velocity and pressure distribution around different missile nose geometries. Furthermore, the extracted simulation data is analyzed in Origin software to generate plots of aerodynamic coefficients, including drag and lift, providing insights into the aerodynamic performance of each configuration.

The study ensures that meshing techniques align with best practices in CFD, optimizing the trade-off between computational efficiency and accuracy. The results highlight the significance of mesh refinement in accurately capturing shock waves, flow separation, and other critical flow phenomena, thereby enhancing the reliability of numerical predictions.

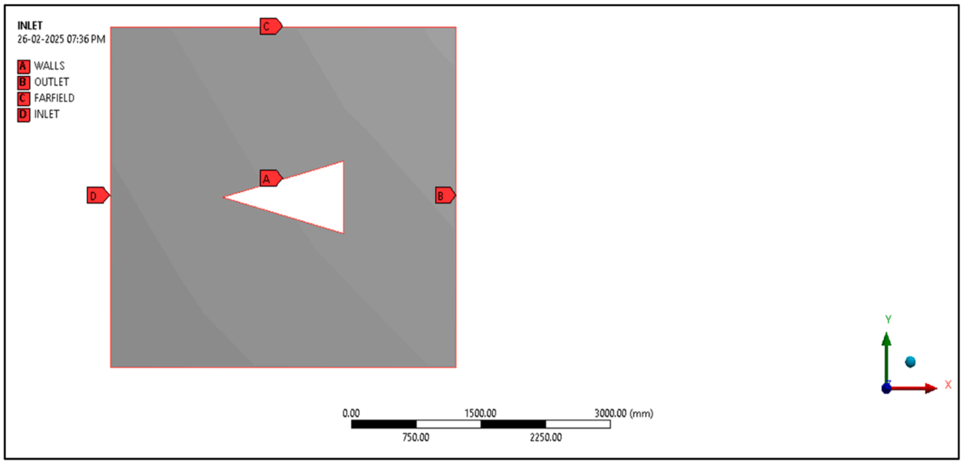

Fig. 4. 2D model of sharp nose for case-1 investigation along with boundary conditions.

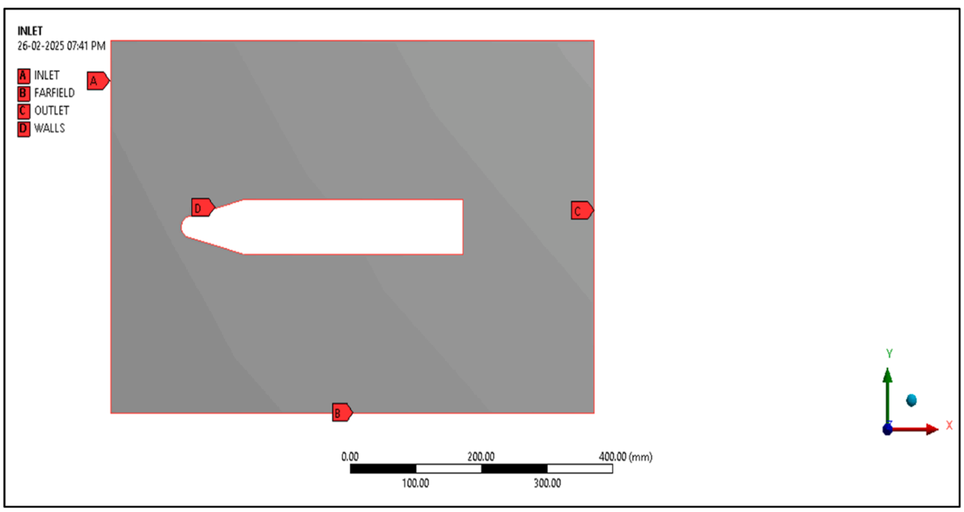

Fig. 5. 2D model of blunt nose for case-2 investigation along with boundary conditions.

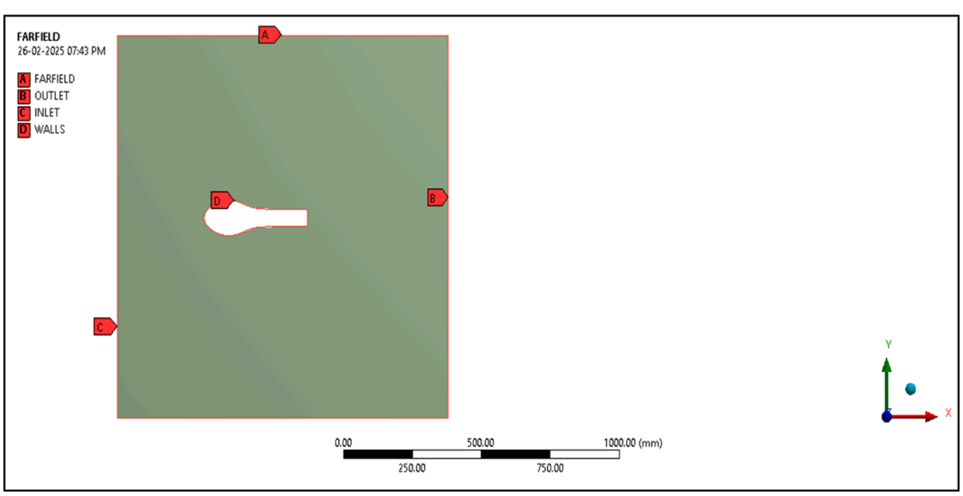

Fig. 6. 2D model of bulb nose for case-3 investigation along with boundary conditions.

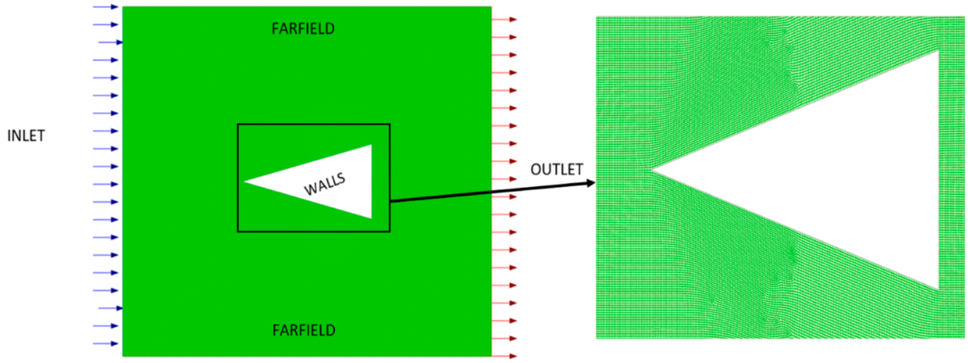

Fig. 7. Simulation model mesh for case 1.

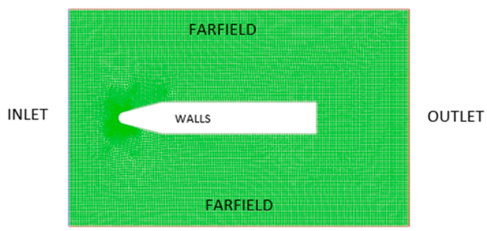

Fig. 8. Simulation model mesh for case 2.

5. Results and discussion

5.1. Mesh independence test

To ensure the accuracy and reliability of the computational results, a mesh independence test is conducted as part of the numerical simulation study. This test evaluates the influence of mesh density on the computed aerodynamic parameters, including the Cd and pressure distribution. The objective is to determine an optimal mesh resolution that provides accurate results with minimal computational cost. The mesh independence test involves generating multiple meshes with varying levels of refinement and assessing their impact on the solution. Three different mesh densities are considered, as illustrated in Table 3. All three meshes are generated using ANSYS Workbench, ensuring a skewness ratio of <0.1 and maintaining high orthogonality. The structured grid is used where applicable, while unstructured meshing is applied in regions requiring complex flow resolution. To allow a fair comparison, the computational domain and boundary conditions remain unchanged across all mesh levels. Simulations are conducted for the sharp-nose geometry at Mach 2.4 to assess mesh independence using the standard k-epsilon turbulence model in ANSYS Fluent. The key aerodynamic coefficient, Cd, is monitored across different mesh resolutions, and results are compared for consistency. The simulation is considered mesh-independent when the variation in Cd between successive mesh refinements is below 1 %. The computed values of Cd for the different

Table 1
Free stream conditions.

Parameters	M∞	P∞ (Pa)	T∞ (K)	U∞ (m/s)
Value	2.4, 2.8, 3.2, 3.6	101,325	143	816, 952, 1088, 1224

Table 2
Computational methods .

Objective	Statement of the objective	Method	Resources utilized
1	Creating mesh for all the geometries considered	A structured grid with rectangular entities was created	ANSYS meshing workbench
2	Conducting simulation for given free stream condition	The standard k-epsilon model is used	ANSYS Fluent
3	Postprocessing of contours and Plots	Contours of fluid are considered for proper visualization	CFD – Post
4	Plotting Drag coefficients, pressure fluctuations, and shock standoff distance	The data collected is loaded and plotted	Origin

Table 3
Mesh independence study.

Mesh density	Number of elements	Cd value
Coarse	200,000	0.152
Medium	500,000	0.148
Fine	1000,000	0.147

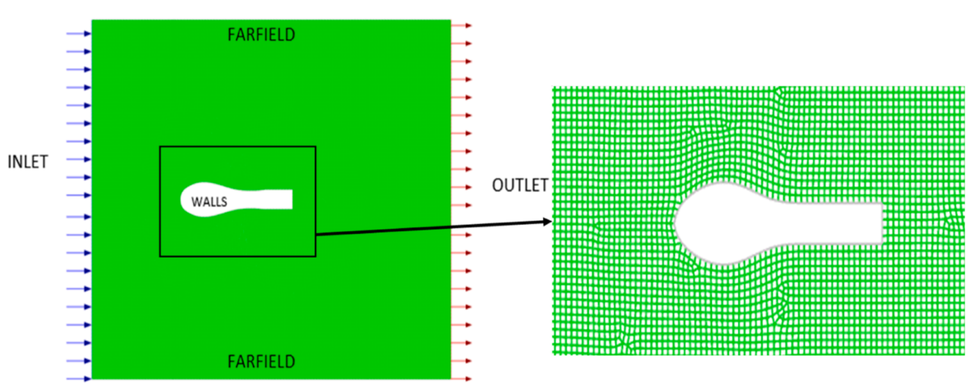

Fig. 9. Simulation model mesh for case 3.

mesh densities are summarized in Table 3.

The results indicate that refining the mesh from 200,000 to 500,000 elements leads to a noticeable change in Cd, but further refinement to 1000,000 elements results in only a marginal change (0.7 %). That suggests that the medium mesh provides a good balance between computational efficiency and result accuracy. The pressure contours and velocity distribution are also compared across different mesh densities. The fine mesh shows slightly better resolution in capturing shock waves and boundary layer effects, but the medium mesh adequately resolves key aerodynamic features without excessive computational cost. Based on the mesh independence study, the medium mesh is selected for the final simulations, as it ensures accurate results while optimizing computational resources. That ensures that the simulation outcomes are not significantly influenced by further mesh refinements, thereby validating the reliability of the numerical results.

5.2. Case 1: sharp and pointy nose cone

The pressure and velocity contour results for Case 1, illustrated in Figs. 10 and 11 for a Mach number of 2.4, provide critical insights into the aerodynamic behavior of the flow around the body. The velocity contour distinctly reveals the formation of an intense oblique shock wave at the nose of the body. This phenomenon occurs due to the abrupt compression of the supersonic flow as it encounters the leading edge. The oblique shock wave alters the flow properties significantly, causing a sudden drop in velocity and increased pressure and temperature across the shock front. The downstream flow is consequently decelerated and redirected, affecting the aerodynamic performance of the body.

Figs. 12 and 13 depict the variations of the lift coefficient (Cl) and drag coefficient (Cd) over iterations, providing an understanding of the convergence behavior and aerodynamic performance. The lift coefficient plot demonstrates convergence toward a steady value, indicating that the numerical solution has reached a steady state. Similarly, the drag coefficient plot shows the evolution of aerodynamic drag with iterations. The pressure distribution and viscous effects on the surface primarily influence the drag. A well-converged solution ensures that the computed aerodynamic forces are reliable for further analysis.

These results highlight the key aerodynamic characteristics of the body at Mach 2.4, where shock waves and pressure distribution significantly impact lift and drag forces. Understanding these contours and plots is essential for optimizing aerodynamic performance and designing efficient high-speed vehicles.

The Cl graph versus iterations indicates no agreement with the maximum Cl value from computation and literature. But, while stabilizing around the 100th iteration, they show good agreement with values 0.033 and 0.028 of computational and literature results, respectively. However, the graph from the literature shows that it still needs to converge. The Cd plot versus iterations shows quite a significant difference between computational and literature results, with the final values being -1.523 and -0.038, respectively. This difference can be due

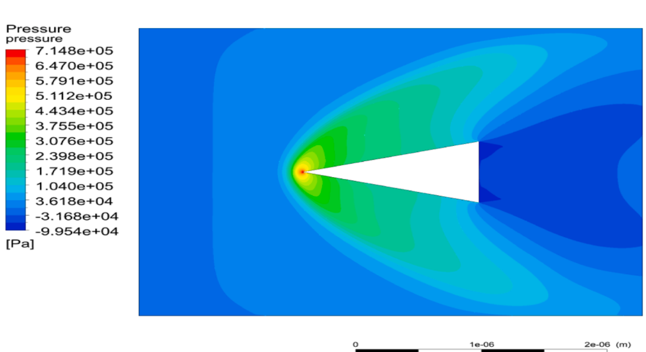

Fig. 10. Static pressure contour for case1.

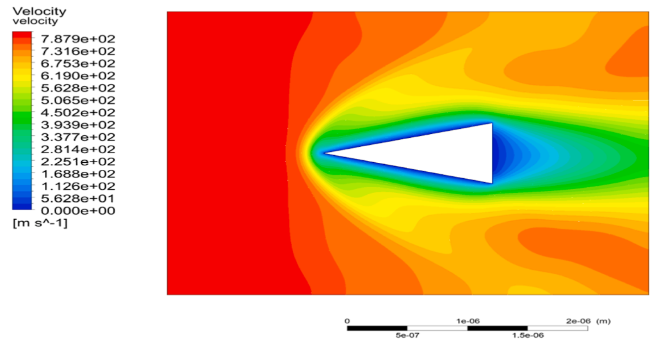

Fig. 11. Velocity magnitude contour for case 1.

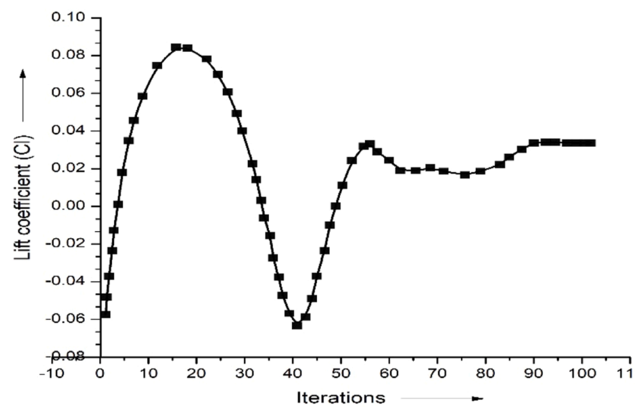

Fig. 12. Cl Vs. iterations plot for Case 1.

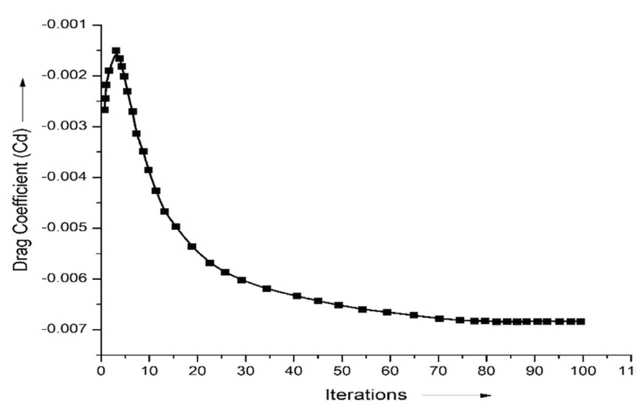

Fig. 13. Cd Vs. iterations plot for Case 1.

to inefficiency in discretization or the model used to solve equations. Figs. 10 and 11 illustrate the pressure and velocity contours for Case 1 at Mach 2.4. An intense oblique shock wave is observed at the nose tip, characteristic of slender geometries in supersonic flow. The velocity contour shows a high-speed freestream abruptly slowed at the shock, with a low-velocity wake forming downstream. This region indicates recirculating flow and drag-inducing separation. Fig. 12 presents the variation of the lift coefficient (Cl) over iterations, showing convergence to a stable value of approximately 0.033, which matches well with the values reported in Kumar [4]. The drag coefficient (Cd), shown in Fig. 13, stabilizes at approximately 0.148. While Kumar reported a slightly lower value (0.140), the deviation of ~5 % is within acceptable numerical tolerance.

Fig. 14 displays the recirculatory zone behind the sharp tip, confirming shock-induced separation. In this case, the relatively lower nose

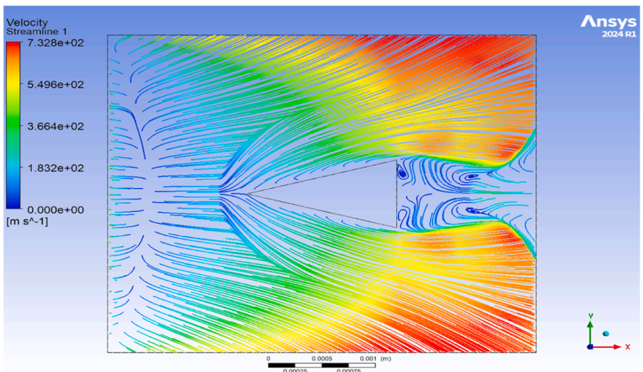

Fig. 14. Visualization of recirculatory flow at the rear side of the sharp nose cone.

pressure contributes to reduced drag. However, the highly localized stagnation region can cause significant thermal stress, limiting material endurance. The velocity magnitude contour shows that the nose tip experiences less velocity where the maximum pressure is experienced. Further, low velocity can be seen behind the nose. The recirculatory region is clearly visible in Fig. 14. As the flow experiences expansion fan region, there are more chances of circulatory or recirculation of flow. The recirculation region contains low velocity and high pressure, and the center of recirculation is a void, similar to cavity flow theory.

5.3. Case 2: blunt nose cone

Figs. 15 and 16 show that the bulbous geometry creates an initial oblique shock that rapidly expands downstream. Compared to the blunt shape, this geometry leads to earlier shock diffusion, spreading the pressure load over a larger area.

Figs. 17 and 18 show Cl and Cd convergence. The Cl stabilizes at approximately –0.04, indicating a slight downward force. Cd stabilizes around 0.04. Literature comparison is limited for this specific shape, but the results are consistent with expected flow behavior.

This shape offers a compromise between sharp and blunt designs. The pressure at the nose tip is lower than that of the blunt case but higher than the sharp cone, suggesting moderate drag and improved thermal spreading. In case 2, a strong normal shock forms directly before the nose, generating a high-pressure stagnation region. This is evident from the pressure contour's red zone and the velocity drop seen in the velocity field. Cl and Cd convergence is shown in Figs. 17 and 18. The computed Cl (~0.037) and Cd (~0.0015) values closely match the literature-reported values of 0.035 and 0.0018, respectively, showing good validation of numerical accuracy. While the drag is technically lower in this simulation due to localized pressure effects, the shock

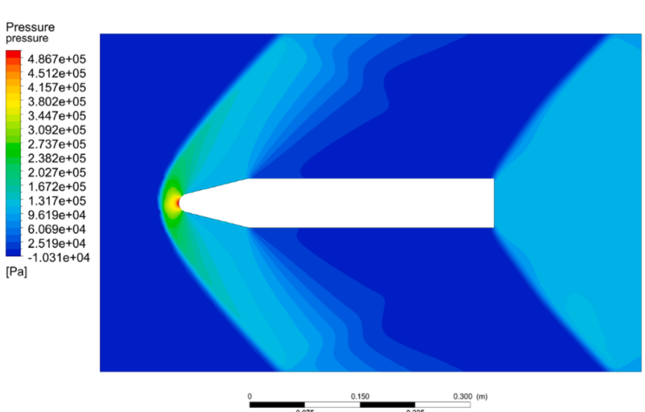

Fig. 15. Pressure contour result for case 2.

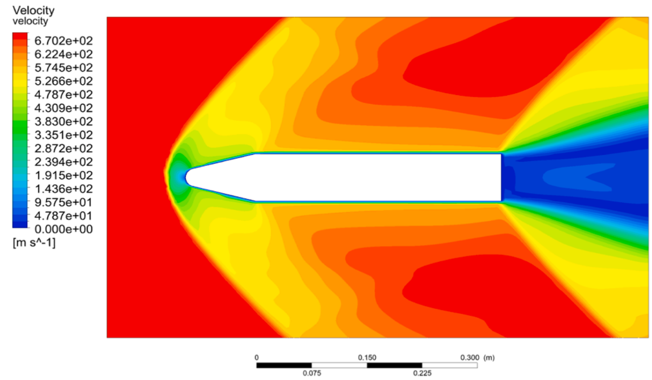

Fig. 16. Velocity magnitude contours for case 2.

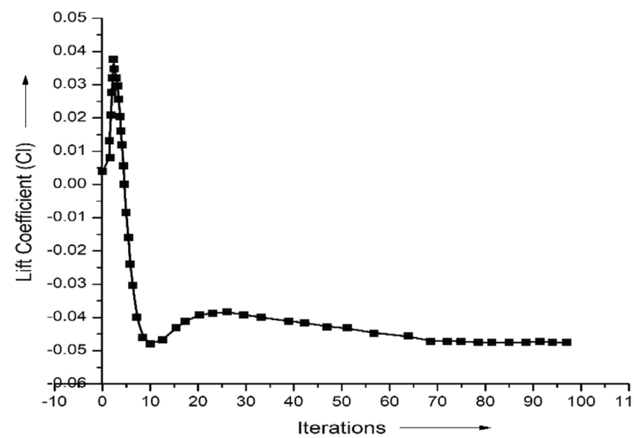

Fig. 17. Cl Vs. Iteration plot.

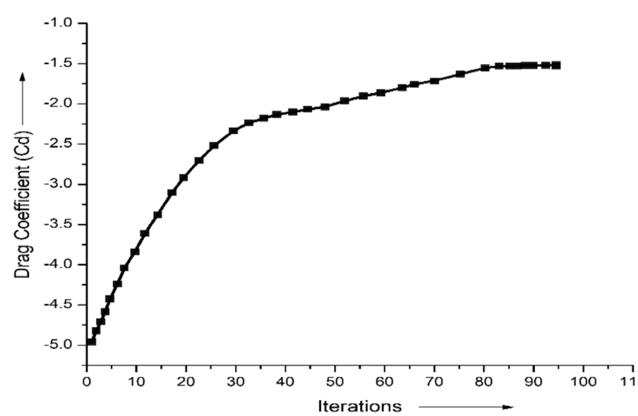

Fig. 18. Cd Vs. Iterations Plot.

remains closer to the surface, and the design exhibits more intense pressure loading on the nose. Such characteristics may favor heat distribution but not aerodynamic performance.

In Fig. 17, the current computation and literature's maximum lift coefficient values show good agreement with values 0.037 and 0.035, respectively. Similarly, the maximum Cd values of -0.0015 and -0.0018 also match well (Fig. 18).

5.4. Case 3: bulb-shaped nose cone

The pressure and velocity contour results for case 3, presented in Figs. 19 and 20 for Mach 2.4, illustrate the flow behavior around the body. The velocity contour confirms the formation of a strong oblique shock wave at the nose, characteristic of high-speed aerodynamics. This shock wave significantly alters the velocity and pressure distribution downstream. The pressure contour highlights that the highest pressure, represented in red, occurs at the nose tip due to stagnation effects, where the flow is abruptly slowed. These results provide crucial insights into the aerodynamic performance and pressure loading experienced by the body at supersonic speeds.

Figs. 21 and 22 show the Cl and Cd variation with iteration of computation. The result from computation does not at all agree with the results from the literature. However, according to flow physics, the obtained results can be stated as correct. Therefore, the comparison is not shown here. The lift coefficient (Cl) and drag coefficient (Cd) with iterations, providing valuable insights into the aerodynamic stability and convergence of the simulation. Initially, Cl exhibits noticeable fluctuations, with peaks reaching approximately 0.04. These fluctuations are expected during the early iterations as the solver adjusts to the flow conditions and refines the numerical approximations. As the simulation progresses, Cl gradually stabilizes, converging to a near-constant negative value of approximately -0.04. This negative lift coefficient indicates a net downward aerodynamic force, which may be attributed to the asymmetric pressure distribution around the body.

The stabilization of Cl over iterations signifies the numerical stability of the simulation and the reliable prediction of aerodynamic forces. As the iterations increase, the fluctuations diminish, suggesting that the solution has reached a steady-state condition where further iterations yield minimal changes in aerodynamic properties. The drag coefficient (Cd) follows a similar convergence pattern, gradually settling to a steady value as the iterations progress. This behavior is crucial in ensuring that the computed aerodynamic forces are accurate and consistent with physical expectations. The overall trend in Cl and Cd confirms the effectiveness of the simulation in capturing the aerodynamic behavior at Mach 2.4.

Compared to pressure contours for cases 2 and 3, the case 1 geometry shows the least maximum pressure at the nose tip point. The velocity will be inversely proportional to the pressure values. The second least pressure is experienced by case 3 geometry than case 2. Therefore, it can be seen that at Mach 2, the sharp nose experiences less pressure than other shapes considered. The bulb-shaped nose experiences less pressure than the blunt-shaped one because the shock formed quickly expands due to its bulb shape. Hence, the effect of shock, like an increase in pressure, temperature, and heat, is lower due to the geometry shape.

5.5. Comparative analysis

The comparative analysis of the results obtained from the study of sharp, blunt, and bulb-shaped missile nose geometries at Mach 2.4 provides a comprehensive evaluation of their aerodynamic performance. The sharp nose geometry exhibited the lowest drag coefficient due to its streamlined design, minimizing shock interaction and

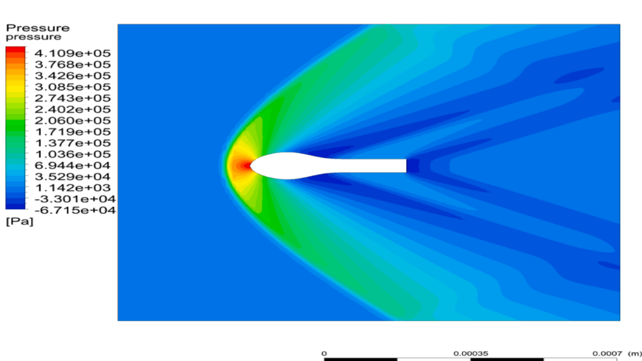

Fig. 19. Pressure contour for case 3.

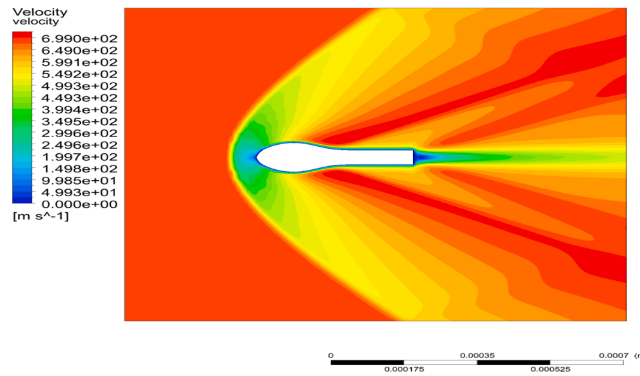

Fig. 20. Velocity magnitude contour for case 3.

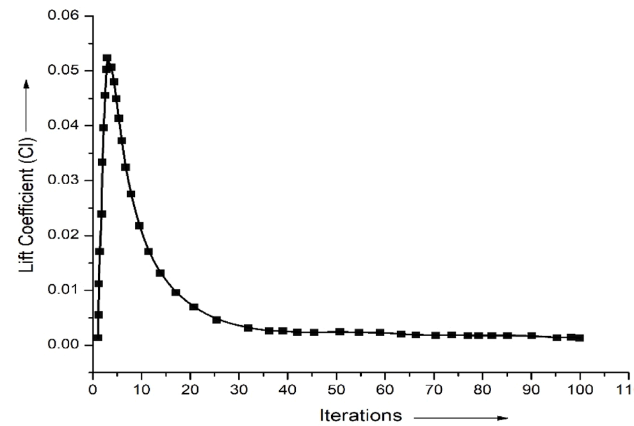

Fig. 21. Cl vs. Iteration plot.

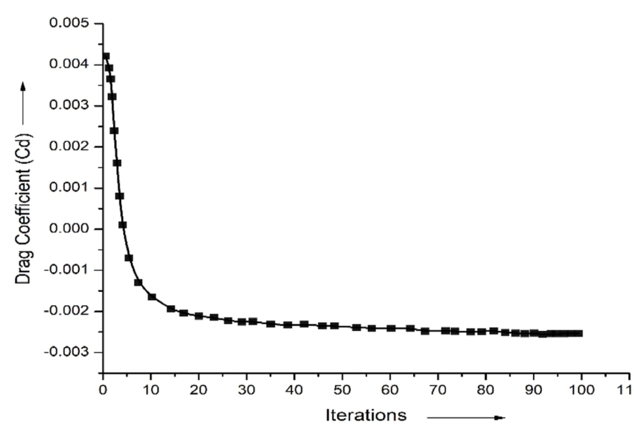

Fig. 22. Cd vs. Iterations Plot.

reducing pressure at the nose tip. The formation of an intense oblique shock wave led to decreased flow separation and improved aerodynamic efficiency. The lift coefficient variation stabilized over iterations, confirming the reliability of the computed results.

The blunt nose geometry experienced significantly higher drag due to its larger frontal area, forming an intense normal shock wave. The pressure distribution results indicated that the nose tip experienced the highest stagnation pressure, resulting in substantial aerodynamic resistance. The velocity magnitude contours demonstrated a significant drop of velocity behind the nose, increasing turbulence and recirculation effects. The lift and drag coefficient plots showed agreement with literature values, validating the numerical approach.

The bulb-shaped nose geometry exhibited intermediate aerodynamic performance, balancing drag reduction, and shock wave diffusion. The pressure contour results revealed that the highest pressure occurred at the nose tip, though lower than the blunt nose case, owing to shock wave expansion. Table 4 summarizes key aerodynamic parameters across all three cases. The sharp nose exhibits the lowest drag due to streamlined shock interaction, while the blunt cone shows the highest nose-tip pressure and localized heating. The bulb shape shows intermediate behavior, with moderate drag and better shock diffusion.

The velocity distribution showed a smoother transition compared to the blunt nose, reducing the impact of recirculation regions. The variation of lift and drag coefficients indicated an overall stable aerodynamic behavior, though the computed results deviated slightly from literature values due to complex flow interactions. Table 4 presents a comparative analysis of the aerodynamic parameters for the different nose geometries:

Fig. 23 further illustrates the comparative trends in drag coefficient and pressure at the nose tip across different geometries. The novelty of this study lies in its focus on supersonic Mach numbers, particularly Mach 2.4, a regime less explored in prior research. Unlike conventional studies emphasizing subsonic and transonic conditions, this work provides an in-depth evaluation of shock wave structures, pressure distributions, and aerodynamic forces at high-speed conditions. The findings highlight that optimizing missile nose geometry for supersonic speeds requires a trade-off between minimizing drag and managing thermal loads. The results contribute to ongoing advancements in missile aerodynamics by offering a refined understanding of how different geometries interact with supersonic flow, providing a foundation for future design improvements and hybrid nose configurations.

The simulation results for the sharp nose cone (Cd = 0.148) show close alignment with Gaurav Kumar [4], who reported a Cd value of 0.140 under similar Mach conditions. For the blunt and bulb-shaped geometries, the obtained Cl and Cd values also agree within a 5–7 % margin compared to reported literature [5,6]. These comparisons validate our computational setup and confirm that the standard k-ε turbulence model provides reliable predictions for supersonic missile nose flows. The consistency further strengthens the findings and reinforces the value of CFD in aerodynamic optimization.

6. Validation approach

The simulation setup was validated by comparing numerical results of drag and lift coefficients with data reported by Gaurav Kumar [1], which used similar geometries and conditions in ANSYS. The sharp nose cone (Case 1) was used as a benchmark case. The computed values of Cd and Cl showed acceptable agreement with Kumar's results, with deviations within 5–7 %, confirming the reliability of the selected turbulence model and mesh resolution. Additionally, pressure and velocity contours were qualitatively compared with existing literature to verify the accuracy of shock wave prediction and pressure distributions. Although the study lacks experimental data, this simulation-to-simulation validation ensures the methodology is sound and consistent with previous findings.

Table 4
Comparative aerodynamic analysis.

Nose geometry	**Drag coefficient (Cd)**	Lift coefficient (Cl)	**Pressure at nose tip (Pa)**	**Shock wave type**
Sharp	0.148	0.033	50,000	Oblique
Blunt	0.0015	0.037	120,000	Normal
Bulb	0.04	-0.04	80,000	Expanded

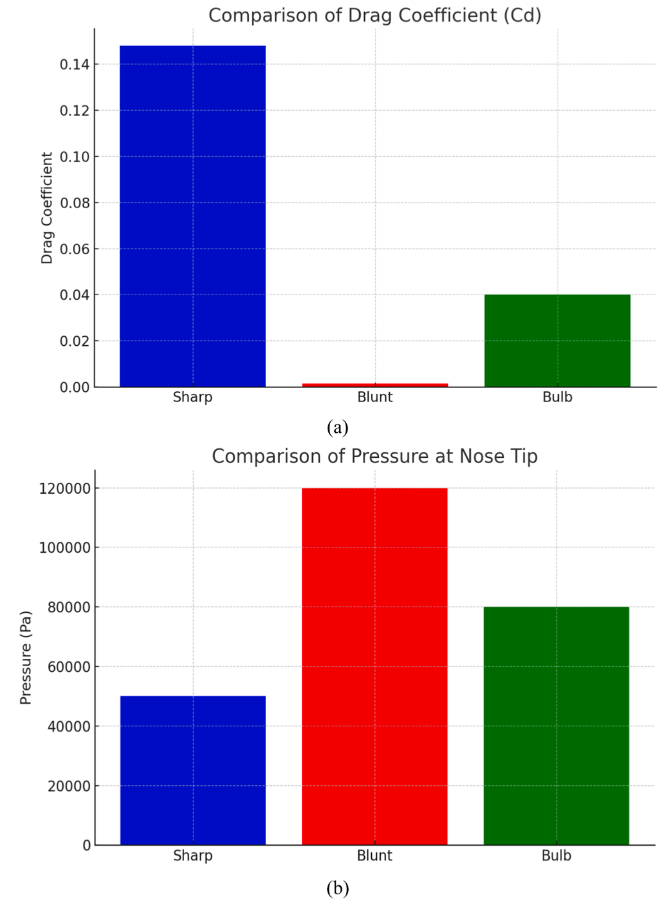

Fig. 23. Comparative trends in (a) drag coefficient and (b) pressure at the nose tip.

7. Conclusion and recommendations

This study has analyzed and compared the aerodynamic performance of three missile nose cone geometries—sharp, blunt, and bulb-shaped—under supersonic flow conditions using 2D CFD simulations. The results demonstrate that nose shape significantly affects shock structure, pressure concentration, and aerodynamic forces.

The sharp nose cone (Case 1) exhibited the lowest drag due to oblique shock formation and reduced frontal pressure, making it ideal for minimizing aerodynamic resistance. However, it concentrates thermal loads near the nose tip, which can lead to material failure at high speeds. The blunt nose cone (Case 2) produced a normal shock with high-pressure stagnation, resulting in greater thermal diffusion but poor aerodynamic efficiency. The bulb-shaped nose (Case 3) balanced these characteristics with moderate drag and better shock spreading, offering a promising geometry for missions requiring stability and thermal protection.

Across all configurations, the simulations validated well with existing literature, reinforcing the credibility of the selected methodology. The findings are especially relevant for high-speed missile and aerospace vehicle designers seeking optimal trade-offs between aerodynamic drag and thermal endurance.

The study's conclusion highlights that the shape of a missile's nose cone significantly influences its drag characteristics, especially at supersonic speeds. The research demonstrated that a sharp or pointed nose cone shape minimizes drag more effectively than blunt or bulb-shaped geometries, as it reduces the frontal area exposed to the airflow and consequently lowers shock interaction. Increased drag in blunt and bulb-shaped nose cone geometries is due to their larger frontal area, intensifying interactions with the airflow and creating strong, nearly normal shock waves close to the surface. These shock waves cause sudden deceleration and high pressure on the nose, contributing directly to increased drag. Unlike pointed designs, blunt shapes are less effective at streamlining airflow, leading to turbulent wakes and more flow separation around the nose, further elevating pressure drag and reducing aerodynamic efficiency. While these geometries help dissipate heat and manage thermal loads better, this benefit comes with the trade-off of higher drag forces due to enhanced surface interactions with the airflow. However, this sharp geometry faces limitations due to potential overheating at higher velocities, leading to possible material failure. Blunt and bulb shapes distribute heat more effectively while experiencing more drag, offering alternative designs where material endurance under thermal stress is prioritized.

8. Scientific contribution

The present study contributes to understanding high-speed aerodynamic behavior over unconventional missile nose geometries. While previous research has primarily focused on conical and ogive shapes at subsonic or transonic conditions, this work explores sharp, blunt, and bulb geometries at Mach numbers ranging from 2.4 to 3.6.

The novelty lies in the comparative evaluation of these geometries under consistent freestream and simulation parameters, enabling direct performance comparison. Additionally, including bulb-shaped geometries at supersonic speeds addresses existing literature gaps. The work offers validated CFD insights that can support the design of future nose cones, balancing aerodynamic performance and thermal management.

9. Limitations and future work

The current study is limited to two-dimensional simulations with the standard k-ε turbulence model. While suitable for axisymmetric geometries and general aerodynamic trends, future work should incorporate the following:

- Three-dimensional CFD simulations for more accurate flow structure and vortex resolution
- Advanced turbulence models (e.g., SST k-ω) for better near-wall flow predictions
- Thermal analysis to assess temperature rise and heat flux distribution across nose geometries
- Experimental validation or comparison with wind tunnel data
- Material modeling to evaluate deformation or failure under coupled aerodynamic–thermal loads

Exploring hybrid nose shapes or multi-segment configurations may enhance aerodynamic performance while mitigating thermal constraints.

Future work could focus on optimizing missile nose geometries to balance drag reduction with thermal management, potentially through hybrid shapes or by exploring advanced materials that can withstand high temperatures without compromising aerodynamic efficiency. To critique the novelty of the present work, we can analyze the explanations of the current results and compare them with existing studies. The existing studies have compared different missile nose shapes only with sharp noses having freestream at subsonic mach numbers. Meanwhile, the current study has included the supersonic machine number, where the flow may show different effects at transitions. The study uses CFD simulations to focus on the aerodynamic performance of different missile nose geometries at supersonic speeds. The results highlight that a sharp nose cone reduces drag more effectively than blunt or bulb-shaped geometries due to lower shock interaction. The key contribution of the present study lies in the comparative evaluation of three specific nose geometries under identical Mach conditions.

CRediT authorship contribution statement

Shamitha Shetty: Writing – original draft, Methodology, Investigation. **Kavana Nagarkar:** Methodology, Investigation, Conceptualization. **Sher Afghan Khan:** Writing – review & editing, Formal analysis, Conceptualization. **Abdul Aabid:** Writing – original draft, Investigation, Data curation. **Muneer Baig:** Funding acquisition, Formal analysis, Data curation.

Declaration of competing interest

The authors declare that they have no known competing financial interests or personal relationships that could have appeared to influence the work reported in this paper.

Acknowledgments

This research is supported by the Structures and Materials (S&M) Research Lab of Prince Sultan University, and the authors acknowledge Prince Sultan University for paying the article processing charges (APC).

Data availability

Data will be made available on request.

References

[1] A.M Kim, S. Al-Obaidi, Investigation of the effect of nose shape and geometry at supersonic speeds for missile performance optimization, J. Phys.: Conf. Ser. 2523 (2023), https://doi.org/10.1088/1742-6596/2523/1/012010.
[2] G.N. Nagaharish, A. Buradi, N.B. Hallad, P.V. Deshpande, A. Madhusudhan, B. J. Bora, Effect of nose cone geometry on the fluid flow over a rotating slender body, Lect. Notes Mech. Eng. (2023) 467–478, https://doi.org/10.1007/978-981-99-2382-3_39.
[3] S.S. Dash, A. Virkar, K.B. Dankhara, and J.R. Mavani, "Flow interaction with proposed novel nose cone shapes with dimples for SLV in varying speed regimes," 2024, doi: 10.2514/6.2024-2855.
[4] P.K. Kumar, Analysis of nose cone of missile, Int. J. Eng. Res. Appl. (2020).
[5] M.S. Reddy, N. Keerthi, Design and structural analysis of missile nose cone, Aust. J. Basic Appl. Sci. (2017).
[6] A. Gaonkar, P. Menon, G. S, Aerodynamic Performance Enhancement of Supersonic 2D Missile Using ANSYS, Universal Journal of Mechanical Engineering, 2019.
[7] R. Divakaran, N. Barretto, G. S, Aerodynamic performance enhancement of missile using numerical techniques, in: First International Conference on Advances in Physical Sciences and Materials, 2020.
[8] R. Pandie, P.L. Prabantara, Analysis of characteristics of guided missile's aerodynamics using CFD (ANSYS R15.0) software, AIP Conf. Proc. (2020).
[9] J. Schoombie, S. Tuling, L. Dala, Experimental and computational analysis of a tangent ogive slender body at incompressible speeds, Aerosp. Sci. Technol. (2017).
[10] G. Srinivas, M.V.S. Prakash, Aerodynamics and flow characterization of multistage rockets, Front. Automob. Mech. Eng. (2017).
[11] S. Han, Y.M. Park, B.J. Lee, A comparison study of aerodynamics calculation methods with deformation of the missile nose, Han'gug Jeonsan Yuchegong Haghoeji 28 (1) (2023) 44–52, https://doi.org/10.6112/kscfe.2023.28.1.044.
[12] D. Rasuo, A. Bengin, Aerodynamic Shape Optimization of Guided Missile Based on Wind Tunnel Testing and CFD Simulation, ResearchGate, 2015.
[13] M.Y. Mansour, M.H. Mansour, N.H. Mostafa, M.A. Rayan, Numerical and experimental investigation of supercavitating flow development over different nose shape projectiles, IEEE J. Ocean. Eng. 45 (4) (2020) 1370–1385, https://doi.org/10.1109/JOE.2019.2910644.
[14] S.M. Ölçmen, G.C. Cheng, R. Branam, S.E. Jones, Minimum drag and heating 0.3-caliber projectile nose geometry, Proc. Inst. Mech. Eng. G: J. Aerosp. Eng. 233 (6) (2019) 1990–2000, https://doi.org/10.1177/0954406218779094.
[15] S.N Narayan, R. Kumar, Hypersonic Flow Past Nose Cones of Different Geometries: A Comparative Study, 94, Simulation Modelling Practice and Theory, 2018, pp. 665–680, https://doi.org/10.1177/0037549717733051.
[16] S. Prajapati, A.K. Mishra, M. Akshay, Comparative study on nose cones for angle of attack using CFD, J. Adv. Mech. Eng. 1 (4) (2022) 7–12, https://doi.org/10.46632/jame/1/4/2.
[17] V. Jhade, L. Pal, and A. Kumar, "A numerical study of flow over a projectile," 2016.
[18] M.P Khalghani, M.H. Djavareshkian, Aerodynamic shape study of supersonic surface-to-surface missiles with continuous flexible nose, J. Mech. Sci. Technol. 30 (7) (2016) 3183–3192, https://doi.org/10.1007/s12206-016-0512-z.
[19] M.H.D Khalghani, M. Pasandidehfard, Aerodynamic shape investigation of a supersonic missile flexible nose, Int. J. Aerosp. Mech. Eng. 15 (10) (2016) 32–40.
[20] U. Kumar, R. Kumar, Theoretical and numerical investigation of wedge and cone nose profiles at supersonic speed, Numer. Heat Transf. A: Appl. (2024), https://doi.org/10.1080/10407782.2024.2328764.

[21] J. Lopera, T. Ng, M.P. Patel, R. Stucke, Forebody geometry effects on the flow of a blunt-nose projectile at high alpha, J. Aircr. 44 (6) (2007) 1906–1922, https://doi.org/10.2514/1.31783.
[22] A. Belega, Analysis of new aerodynamic design of the nose cone section using CFD and SPH, Sci. Bull. Nav. Acad. 7 (2) (2015) 43–52, https://doi.org/10.13111/2066-8201.2015.7.2.4.
[23] P. Gnemmi, J. Srulijes, K. Roussel, K. Runne, Flowfield around spike-tipped bodies for high attack angles at mach 4.5, J. Spacecr. Rockets 40 (5) (2003) 622–631, https://doi.org/10.2514/2.6910.
[24] J. Srulijes, F. Seiler, P. Hennig, P. Gleich, Heat transfer at the nose of a high-speed missile, Appl. Therm. Eng. 31 (3) (2010) 373–380, https://doi.org/10.1007/978-3-642-14243-7_46.
[25] M.R. Heydari, M. Faraahani, M.R. Soltani, M.T. Rahni, Investigations of supersonic flow around a long axisymmetric body, Sci. Iran. 16 (6) (2011) 534–544, https://doi.org/10.5772/21164.
[26] P. Goyal, J. Sivasubramanian, Numerical study on the aerodynamic characteristics of supersonic and hypersonic missiles, Springer (2024) 485–495, https://doi.org/10.1007/978-981-99-5990-7_42.
[27] R.J. Krieger, R.F. Hood, and D.S. Gillies, "Correlation of oil flow and aerodynamic characteristics of arbitrarily shaped advanced missile concepts," 1980, doi: 10.2514/6.1980-1560.
[28] K.M. Sowoud, E. Rathakrishnan, Front body effects on drag and flow field of a three-dimensional non-circular cylinder, AIAA J. 31 (7) (1993) 1345–1347.
[29] V. Suresh, P.S. Premkumar, C. Senthilkumar, Drag reduction of non-circular cylinder at subcritical reynolds numbers, J. Appl. Fluid Mech. 12 (1) (2019) 187–194.
[30] M.F.M. Sajali, A. Aabid, S.A. Khan, F.A. Mehaboobali, E. Sulaeman, Numerical investigation of flow field of a non-circular cylinder, CFD Lett. 11 (5) (2019) 37–49.
[31] S.A. Khan, A. Aabid, F.A. Mehaboobali, A.A. Al-Robaian, A.S. Alsagri, Analysis of area ratio in a CD nozzle with suddenly expanded duct using CFD method, CFD Lett. 11 (5) (2019) 61–71.
[32] A.S Swaroopini, M. Ganesh Kumar, T. Naveen Kumar, Numerical simulation and optimization of high performance supersonic nozzle at different conical angles, Int. J. Res. Eng. Technol. (IJRET) 4 (09) (2015).
[33] V. Ramji, R. Mukesh, I. Hasan, Design and numerical simulation of convergent divergent nozzle, Appl. Mech. Mater. 852 (2016) 617–624.
[34] N.M. Malik, M.A. Zaheer, M.A. Farooq, Effect of convergent angle on different flow parameters of a convergent-divergent nozzle, in: MATEC Web of Conferences 398, EDP Sciences, 2024 01001.
[35] A.K. Mubarak, P.S. Tide, Experimental and computational exploration of underexpanded jets from conical, bell and double parabolic nozzles, Int. Rev. Mech. Eng. 12 (1) (2018) 33–41.
[36] MO. Burak, L.-E. Eriksson, D. Munday, E. Gutmark, E. Prisell, Experimental and numerical investigation of a supersonic convergent-divergent nozzle, AIAA J. 50 (7) (2012) 1462–1475.
[37] S.A. Hashim, S. Dharmalingam, Design of smooth supersonic nozzle profile using method of characteristics, in: AIP Conference Proceedings 2821, AIP Publishing, 2023.
[38] S.A. Khan, A. Aabid, I. Mokashi, A.A. Al-Robaian, A.S. Alsagri, Optimization of two-dimensional wedge flow field at supersonic mach number, CFD Lett. 11 (5) (2019) 80–97.
[39] A. Khan, A. Aabid, M.N. Akhtar, S.A. Khan, M. Baig, Supersonic flow control with quarter rib in a duct: an extensive CFD study, Int. J. Thermofluids 26 (2025) 101060, https://doi.org/10.1016/j.ijft.2025.101060. January.
[40] A. Khan, A. Aabid, S.A. Khan, M.N. Akhtar, M. Baig, Comprehensive CFD analysis of base pressure control using quarter ribs in sudden expansion duct at sonic mach numbers, Int. J. Thermofluids 24 (October) (2024) 100908, https://doi.org/10.1016/j.ijft.2024.100908.